Aalto University

OPEN ACCESS

This is an electronic reprint of the original article.
This reprint may differ from the original in pagination and typographic detail.

Morozova, D.A.; Larionov, V.M.; Troitsky, I.S.; Jorstad, S.G.; Marscher, A.P.; Gómez, J.L.; Blinov, D.A.; Efimova, N.V.; Hagen-Thorn, V.A.; Hagen-Thorn, E.I.; Joshi, M.; Konstantinova, T.S.; Kopatskaya, E.N.; Larionova, L.V.; Larionova, E.G.; Lähteenmäki, A.; Tammi, J.; Rastorgueva-Foi, E.; McHardy, I.; Tornikoski, M.; Agudo, I.; Casadio, C.; Molina, S.N.; Volvach, A.E.; Volvach, L.N.

The Outburst of the Blazar S4 0954+658 in 2011 March-April

Published in:
The Astrophysical Journal

DOI:
10.1088/0004-6256/148/3/42

Published: 01/01/2014

Document Version
Publisher's PDF, also known as Version of record

Please cite the original version:
Morozova, D. A., Larionov, V. M., Troitsky, I. S., Jorstad, S. G., Marscher, A. P., Gómez, J. L., Blinov, D. A., Efimova, N. V., Hagen-Thorn, V. A., Hagen-Thorn, E. I., Joshi, M., Konstantinova, T. S., Kopatskaya, E. N., Larionova, L. V., Larionova, E. G., Lähteenmäki, A., Tammi, J., Rastorgueva-Foi, E., McHardy, I., ... Volvach, L. N. (2014). The Outburst of the Blazar S4 0954+658 in 2011 March-April. *The Astrophysical Journal*, *148*(3). https://doi.org/10.1088/0004-6256/148/3/42

This material is protected by copyright and other intellectual property rights, and duplication or sale of all or part of any of the repository collections is not permitted, except that material may be duplicated by you for your research use or educational purposes in electronic or print form. You must obtain permission for any other use. Electronic or print copies may not be offered, whether for sale or otherwise to anyone who is not an authorised user.

The Astronomical Journal, 148:42 (9pp), 2014 September doi:10.1088/0004-6256/148/3/42
© 2014. The American Astronomical Society. All rights reserved. Printed in the U.S.A.

THE OUTBURST OF THE BLAZAR S4 0954+658 IN 2011 MARCH–APRIL

D. A. Morozova[1], V. M. Larionov[1,2,3], I. S. Troitsky[1], S. G. Jorstad[1,4], A. P. Marscher[4], J. L. Gómez[5], D. A. Blinov[1,6], N. V. Efimova[1,3], V. A. Hagen-Thorn[1,2], E. I. Hagen-Thorn[1,3], M. Joshi[4], T. S. Konstantinova[1], E. N. Kopatskaya[1], L. V. Larionova[1], E. G. Larionova[1], A. Lähteenmäki[7,8], J. Tammi[7], E. Rastorgueva-Foi[7], I. McHardy[9], M. Tornikoski[7], I. Agudo[4,5,10], C. Casadio[5], S. N. Molina[5], A. E. Volvach[11], and L. N. Volvach[11]

[1] Astronomical Institute of St. Petersburg State University, Universitetsky Pr. 28, Petrodvorets, 198504 St. Petersburg, Russia; comitcont@gmail.com
[2] Isaac Newton Institute of Chile, St. Petersburg Branch, St. Petersburg, Russia
[3] Pulkovo Observatory, Russian Academy of Sciences, Pulkovskoe sh. 65, 196140 St. Petersburg, Russia
[4] Institute for Astrophysical Research, Boston University, 725 Commonwealth Avenue, Boston, MA 02215-1401, USA; jorstad@bu.edu
[5] Instituto de Astrofísica de Andalucía, CSIC, Apartado 3004, E-18080 Granada, Spain
[6] Department of Physics, University of Crete, 71003 Heraklion, Greece
[7] Aalto University Metsähovi Radio Observatory, Metsähovintie 114,FI-02540 Kylmälä, Finland
[8] Department of Radio Science and Engineering, Aalto University PL 13000, FI-00076 Aalto, Finland
[9] Department of Physics and Astronomy, University of Southampton, Southampton SO17 1BJ, UK
[10] Joint Institute for VLBI in Europe, Postbus 2, NL-7990 AA Dwingeloo, The Netherlands
[11] Radio Astronomy Laboratory of the Crimean Astrophysical Observatory, Katsiveli, Crimea 98688, Ukraine
Received 2013 December 9; accepted 2014 May 29; published 2014 July 22

ABSTRACT

We present the results of optical (R-band) photometric and polarimetric monitoring and Very Long Baseline Array imaging of the blazar S4 0954+658, along with *Fermi* γ-ray data during a multi-waveband outburst in 2011 March–April. After a faint state with a brightness level $R \sim 17.6$ mag registered in the first half of 2011 January, the optical brightness of the source started to rise and reached ∼14.8 mag during the middle of March, showing flare-like behavior. The most spectacular case of intranight variability was observed during the night of 2011 March 9, when the blazar brightened by ∼0.7 mag within 7 hr. During the rise of the flux, the position angle of the optical polarization rotated smoothly over more than 300°. At the same time, within 1σ uncertainty, a new superluminal knot appeared with an apparent speed of $19.0 \pm 0.3c$. We have very strong evidence that this knot is associated with the multi-waveband outburst in 2011 March–April. We also analyze the multi-frequency behavior of S4 0954+658 during a number of minor outbursts from 2008 August to 2012 April. We find some evidence of connections between at least two additional superluminal ejecta and near-simultaneous optical flares.

Key words: BL Lacertae objects: individual (S4 0954+658) – galaxies: active – galaxies: jets – polarization

Online-only material: color figures, extended figure, machine-readable and VO tables

1. INTRODUCTION

The blazar S4 0954+658 ($z = 0.367$) is a well-studied BL Lac object at optical wavelengths. Its optical variability was analyzed by Wagner et al. (1993), who found large amplitude variations (of ∼100%) on timescales as short as one day. Raiteri et al. (1999) presented a comprehensive study of the optical and radio variability of the source during 1994–1998. They detected large amplitude intranight variations. An investigation of $B-R$ color variations allowed them to conclude that mid- and long-term brightness variations of the source are not associated with spectral variability. Gabuzda et al. (2000, and references therein) analyzed the radio morphology of S4 0954+658 and showed that the jet is bent on both parsec and kiloparsec jet scales. They also found substantial intranight polarization variability of the radio core at 5 GHz. Kudryavtseva et al. (2010) have found several moving components in the jet at 22 GHz with a mean velocity $4.9 \pm 0.4c$. However, the kinematics of the parsec-scale jet of S4 0954+658 is poorly studied, especially at 43 GHz.

According to Mukherjee et al. (1995), γ-ray emission of S4 0954+658 first was detected by EGRET in 1993. S4 0954+658 was also detected by the *Fermi* Large Area Telescope (LAT) according to the *Fermi* first and second catalogs of γ-ray bright sources (Abdo et al. 2010; Nolan et al. 2012). In this paper, we present a detailed study of the optical outburst of S4 0954+658 in 2011 March–April (Larionov et al. 2011b) along with an analysis of the γ-ray variability and behavior of the innermost radio jet at 43 GHz. Preliminary results of our observations have been described by Larionov et al. (2011a).

2. OBSERVATIONS AND DATA REDUCTION

The observations reported here were collected as a part of a long-term multi-wavelength study of a sample of γ-ray bright blazars. An overview of this program is given by Marscher (2012).

2.1. Optical Observations

We carry out optical *BVRI* observations at the 70 cm AZT-8 reflector of the Crimean Astrophysical Observatory, and 40 cm LX-200 telescope in St. Petersburg, Russia. The telescopes are equipped with identical photometers–polarimeters based on ST-7 CCDs. We perform observations in photometric and polarimetric modes at the 1.8 m Perkins telescope of Lowell Observatory (Flagstaff, AZ) using the PRISM camera and at the 2.2 m telescope of the Calar Alto Observatory (Almería, Spain) within the MAPCAT program.[12] Photometric measurements in R band are supplemented by observations at the 2 m Liverpool Telescope at La Palma, Canary Islands, Spain. Polarimetric observations at the AZT-8, Perkins, and Calar Alto telescopes are carried out in the Cousins R band, while at the LX-200

[12] http://www.iaa.es/∼iagudo/research/MAPCAT/MAPCAT.html

Table 1
Photometry and Polarimetry of S4 0954+658 During 2011 April–May Outburst

RJD (days)	R (mag)	σR (mag)	p (%)	σp (%)	EVPA (°)	σEVPA (°)	Telescope
55577.4520	17.105	0.014	15.57	0.44	172.5	0.1	CAHA
55588.5160	17.182	0.016	15.48	1.12	163.1	2.1	AZT-8+ST7
55601.4340	16.924	0.010	12.55	0.70	162.2	1.6	AZT-8+ST7
55603.9170	16.985	0.007	13.54	0.57	148.3	1.2	Perkins
55604.3090	16.896	0.054	13.82	3.60	180.1	7.5	LX-200
55604.8940	16.987	0.012	11.84	1.31	146.8	3.2	Perkins
55605.8860	16.869	0.010	12.05	0.02	148.8	0.0	Perkins
55607.3730	16.980	0.026	17.48	2.05	171.8	3.4	AZT-8+ST7
55608.2500	16.901	0.069	9.01	3.86	218.1	12.3	LX-200
55609.3790	16.904	0.107	22.39	6.46	133.0	8.3	LX-200

Note. RJD = JD-2400000.0.

(This table is available in its entirety in machine-readable and Virtual Observatory (VO) forms in the online journal. A portion is shown here for guidance regarding its form and content.)

telescope they are performed in white light, with effective wavelength close to R band.

The Galactic latitude of S4 0954+658 is 43° and A_V = 0.38 mag, so that the interstellar polarization (ISP) in this direction is less than 1%. To correct for the ISP, the mean relative Stokes parameters of nearby stars were subtracted from the relative Stokes parameters of the object. This accounts for the instrumental polarization as well, under the assumption that the radiation of the stars is unpolarized. The errors in the degree of polarization, P, are less than 1% (in most cases less than 0.5%), while the electric vector position angle (EVPA), χ, is determined with an uncertainty of 1°–2°. The photometric errors do not exceed 0.02 mag. Photometry and polarimetry of the source during the flare are presented in Table 1.

2.2. *Gamma-Ray Observations*

We derive γ-ray flux densities at 0.1–200 GeV by analyzing data from *Fermi*-LAT, provided by the Fermi Science Space Center using the standard software (Atwood et al. 2009). We have constructed γ-ray light curves with a binning size of seven days, with a detection criterion that the maximum-likelihood test statistic (TS) should exceed 10.0. Although the γ-ray flux fell below the detection limit during most of the period of our observations ($\leqslant 5 \times 10^{-7}$ photons cm^{-2} s^{-1}), there are a number of positive γ-ray detections that are interesting to compare with behavior of the source at other wavelengths.

2.3. *Single-dish Radio Observations*

We use 37 GHz observations obtained with the 13.7 m telescope at the Metsähovi Radio Observatory of Aalto University, Finland. The flux density calibration is based on observations of DR 21, with 3C 84 and 3C 274 used as secondary calibrators. A detailed description of the data reduction and analysis is given in Teräsranta et al. (1998). These data are supplemented by observations carried out at the 22 m RT-22 radio telescope of the Crimean Astrophysical Observatory at 36.8 GHz. In this case, the sources 2037+421, 1228+126, and 2105+420 are used for the flux density calibration. A detailed description of the data reduction and analysis can be found in Nesterov et al. (2000).

2.4. *Very Long Baseline Array Observations*

The BL Lac object S4 0954+658 is monitored monthly by the Boston University (BU) group with the Very Long Baseline

Table 2
Polarization Properties of Knots on VLBA Images

MJD	Knot	Flux (Jy)	p (%)	χ (°)	Date
55724.5	K8	0.10	27.4	146.2	2011 Jun 12
55763.5	...	0.12	19.0	135.0	2011 Jul 21
55796.5	...	0.15	18.7	116.8	2011 Aug 23
55820.5	...	0.08	23.2	117.3	2011 Sep 16
55850.5	...	0.08	23.8	122.6	2011 Oct 16
55897.5	...	0.11	15.4	144.8	2011 Dec 2

Note. MJD = JD − 2400000.5.

(This table is available in its entirety in machine-readable and Virtual Observatory (VO) forms in the online journal. A portion is shown here for guidance regarding its form and content.)

Array (VLBA) at 43 GHz within a sample of bright γ-ray blazars.[13] The VLBA data are calibrated and imaged in the same manner as discussed in Jorstad et al. (2005). We have constructed total and polarized images at 33 epochs from 2010 August to 2012 April. Each image in the Stokes I, Q, and U parameters was fit by a model consisting of a number of components with circular Gaussian brightness distributions. Identification of components in the jet across epochs is based on analysis of their flux, position angle, distance from the core, size, degree of polarization, and EVPA. During this period, we have identified 12 components, A1, K1, K2, K3, K4, K5, K6, K7, K8, K9, K10, K11, in addition to the core, A0. The core is a stationary feature located at the southern end of the portion of the jet that is visible at 43 GHz. We have computed kinematic parameters of knots (the proper motion, velocity, and acceleration) by fitting the (x, y) positions of a component over epochs by different polynomials of the order of 1–3, in the same manner as described in Jorstad et al. (2005). The method produces uncertainties of polynomial coefficients with an assumption that the true value lies with probability W within the confidence region around the estimated value ($W = 0.95$ is applied). The ejection time of a component is the extrapolated time of coincidence of the position of a moving knot with the core in the VLBA images, and $T_{\rm eject}$ is the average of $T_{\rm xeject}$ and $T_{\rm yeject}$ weighted by their uncertainties, which are calculated using uncertainties of the polynomial coefficients.

Table 2 lists for the core and each superluminal knot the flux, fractional polarization level, p, and EVPA, χ. Table 3 lists for each superluminal knot the apparent speed, $\beta_{\rm app}$, acceleration, if detected ($\dot{\mu}_{||}$ and $\dot{\mu}_{\perp}$, along and perpendicular to the jet, respectively), mean position angle with respect to the core, $\langle\Theta\rangle$, and extrapolated time of zero separation from the core, $T_{\rm eject}$.

3. RESULTS AND DISCUSSION

3.1. *Optical Polarization Analysis*

Figure 1 displays the entire set of optical photometric and polarimetric data collected by our team during 2008–2011. The blazar shows prominent activity during the period covered by our observations, with the R-band amplitude of variations exceeding 2 mag and a record level of P exceeding 40%. Even on such an active background, the outburst, which started in early 2011, is quite prominent. An enlargement of the event is shown in Figure 2.

Unlike all of the previous years, starting from the end of 2011 February, a smooth rotation of χ (Figure 2, bottom panel)

[13] http://www.bu.edu/blazars

Table 3
Kinematic Parameters of the VLBI Knots

Knot	N	μ	$\beta_{\rm app}$	$T_{\rm eject}$	$\dot{\mu}_{\perp}$	$\dot{\mu}_{\parallel}$	$\langle\Theta\rangle$
K1	10	0.59 ± 0.01	13.02 ± 0.30	54650.0 ± 15	-0.44 ± 0.02	-0.78 ± 0.03	-26.9 ± 5.47
K2	16	0.37 ± 0.01	8.24 ± 0.02	54883.5 ± 15	...	...	-49.0 ± 7.7
K3	21	0.32 ± 0.02	6.99 ± 0.42	55091.6 ± 30	-0.18 ± 0.01	-0.40 ± 0.01	-20.2 ± 6.6
K4	6	0.61 ± 0.06	13.53 ± 1.42	55184.7 ± 20.6	...	...	-14.3 ± 1.5
K5	5	0.69 ± 0.05	15.14 ± 1.12	55349.5 ± 14.1	...	...	-16.7 ± 2.3
K6	3	0.58 ± 0.01	12.75 ± 0.17	55450.4 ± 15	...	...	-21.7 ± 1.4
K7	3	0.87 ± 0.06	19.24 ± 1.31	55564.4 ± 16.9	...	...	-27.2 ± 0.68
K8	8	0.86 ± 0.01	18.95 ± 0.28	55639.1 ± 15	-1.69 ± 0.06	-0.23 ± 0.06	-25.4 ± 6.4
K9	5	0.78 ± 0.06	17.22 ± 1.39	55704.5 ± 15	...	...	-8.4 ± 4.4
K10	4	1.20 ± 0.07	26.61 ± 1.58	55827.2 ± 26.8	...	...	-24.1 ± 3.1
K11	4	0.92 ± 0.04	20.19 ± 0.91	55871.9 ± 15	...	...	-14.6 ± 2.6

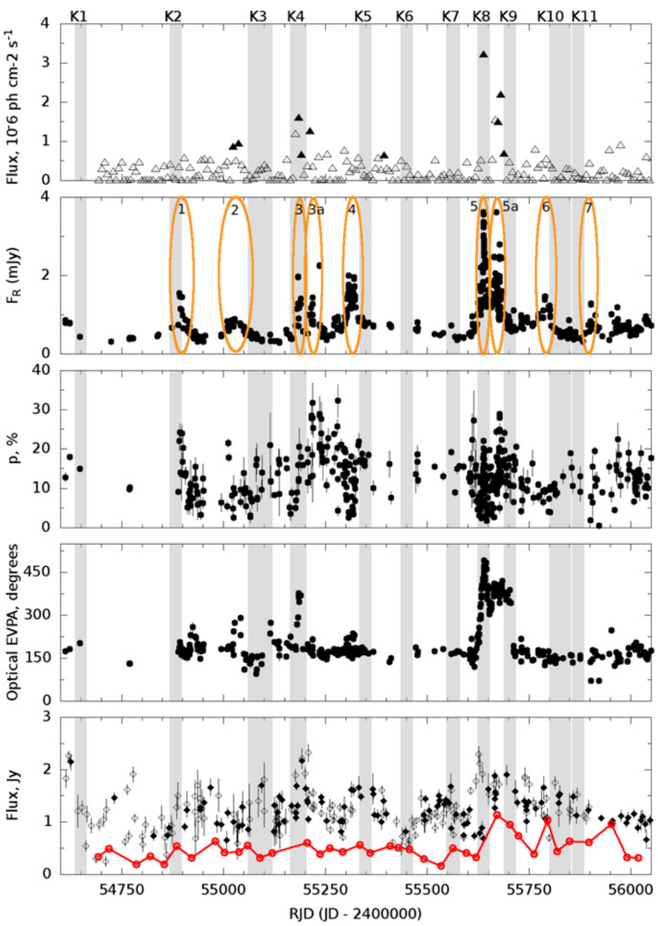

Figure 1. From top to bottom: γ-ray light curve (open triangles are the upper limits); optical (R-band) light curve; fractional polarization vs. time; position angle of polarization vs. time; light curve of the very long baseline interferometry (VLBI) core at 43 GHz (open circles); and light curve from the whole source at 37 GHz (filled diamonds) and 35 GHz (open diamonds). The vertical bars show the times of ejection of superluminal knots within 1σ uncertainty.

(A color version of this figure is available in the online journal.)

with an amplitude of $\sim 330^{\circ}$ is prominent. We see a steady rotation of $\chi \sim 13.3$ mag day^{-1} during 2011 March. The rotation stops at RJD 55643 (2011 March 22), near the peak of the R-band outburst. After that, only minor changes of EVPA are observed, despite continued strong variability of the flux density and fractional polarization. After RJD $\sim$ 55660, the EVPA rotates back to a "quiescent" state ($\sim 0^{\circ}$).

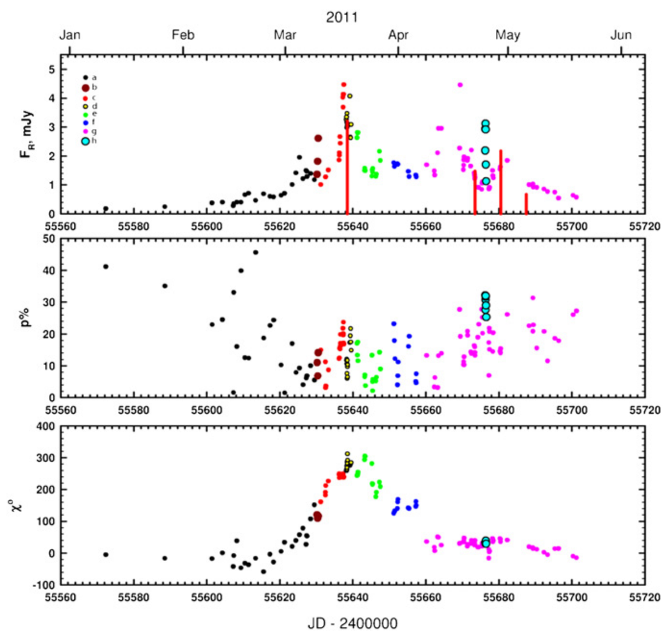

Figure 2. Optical flux density (corrected for Galactic extinction), fractional polarization, and position angle of polarization in R band vs. time in 2011 January–May; magnified symbols refer to the nights with violent intranight variability, colors designate sections of the data with different Stokes parameter behavior (see Table 4). Red vertical bars in the upper panel mark positive *Fermi*-LAT detections; a bar's height is proportional to the γ-ray flux.

(A color version of this figure is available in the online journal.)

During two nights, on March 9 and April 24, we observed violent intranight variability, ~ 0.7 mag within 7 hr and ~ 1.0 mag within 5 hr, respectively, accompanied by synchronous changes in the fractional polarization (marked by the magnified symbols in Figure 2). The fractional polarization varied from 5.8% to 12.6% on March 9 and from 19.8% to 28.9% on April 24. These are the fastest flux and polarization changes recorded for this source in the published literature.

Following Hagen-Thorn & Marchenko (1999), we plotted (Q versus I) and (U versus I) Stokes polarization parameters (see Figure 3) and found that the entire data set can be split into sections with its own behavior in (I, Q, U) parameter space. We mark these sections with different colors in Figure 3 and apply the same colors to the data plotted in Figure 2.

The regression lines in Figure 3 represent components, each with constant parameters of polarization, $P_{\rm comp}$ and $\chi_{\rm comp}$, while its total and polarized fluxes vary. There are eight different components with respect to the Stokes parameters behavior.

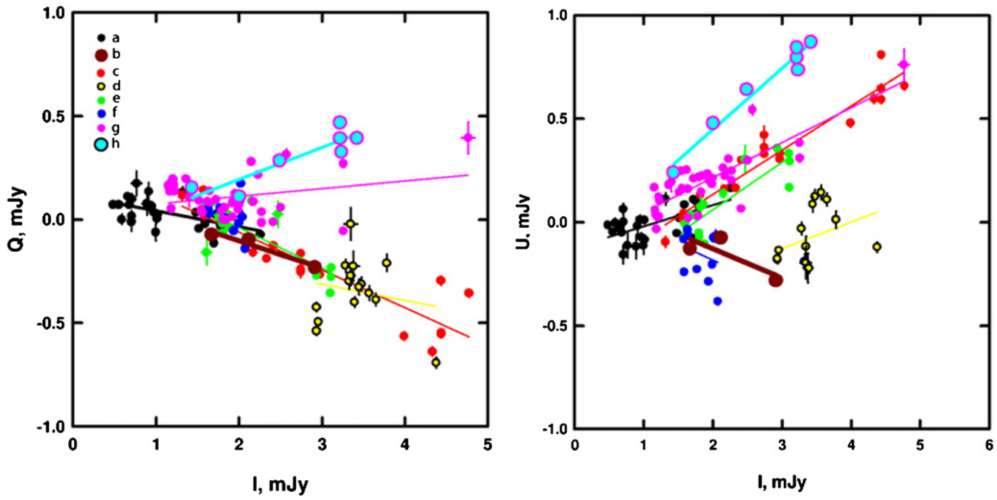

Figure 3. Absolute Stokes parameter variation during 2011 January–April; left: Stokes Q vs. I; right: Stokes U vs. I. Different colors refer to different stages of the evolution in (I, Q, U) parameter space (see Table 4).

(A color version of this figure is available in the online journal.)

Table 4
Optical Polarization Parameters of the Variable Sources

Name	RJD	p (%)	σp (%)	χ (°)	$\sigma \chi$ (°)
a	55572−55629	12.66	1.91	−26.8	4.2
b	55630	19.24	5.18	113.3	7.4
c	55631−55637	27.79	1.22	−24.5	1.2
d	55638−55639	15.26	9.00	−24.7	17.0
e	55641−55647	30.00	2.83	31.3	2.6
f	55651−55657	17.35	11.22	42.3	17.8
g	55660−55701	18.08	1.24	31.2	1.9
h	55676	33.05	2.14	17.0	1.8

Since these components are variable in flux, we will refer to them as variable sources. We note that the regression lines tend to converge on the locus of points corresponding to the pre-outburst values of the Stokes parameters. This implies that one of the components, probably responsible for the flux and polarization of S4 0954+658 before the outburst, has constant Stokes parameters. We estimate the constant source's parameters as $R = 17.8$ (corresponding to flux density of 0.308 mJy after correction for interstellar extinction), $p = 15\%$ and $\chi = -6°$. We assume that the component should contribute the same amount of the total and polarized flux during the outburst as well. Hence, we subtract its contribution from the Stokes parameters of S4 0954+685 to get the radiation parameters of the variable sources. These are listed in Table 4.

We use the technique developed by Hagen-Thorn (see, e.g., Hagen-Thorn et al. 2008, and references therein) to analyze the color variability of S4 0954+65. If the variability is caused only by the flux variation but the relative spectral energy distribution (SED) remains unchanged, then in n-dimensional flux space $\{F_1, \ldots, F_n\}$ (n is the number of spectral bands used in multicolor observations) the observational points must lie on straight lines. The slopes of these lines are the flux ratios for different pairs of bands as determined by the SED. With some limitations, the opposite is also true: a linear relation between observed fluxes at two different wavelengths during some period of flux variability implies that the slope (flux ratio) does not change. Such a relation for several bands would indicate that the relative SED of the variable source remains steady and can be derived from the slopes of the lines.

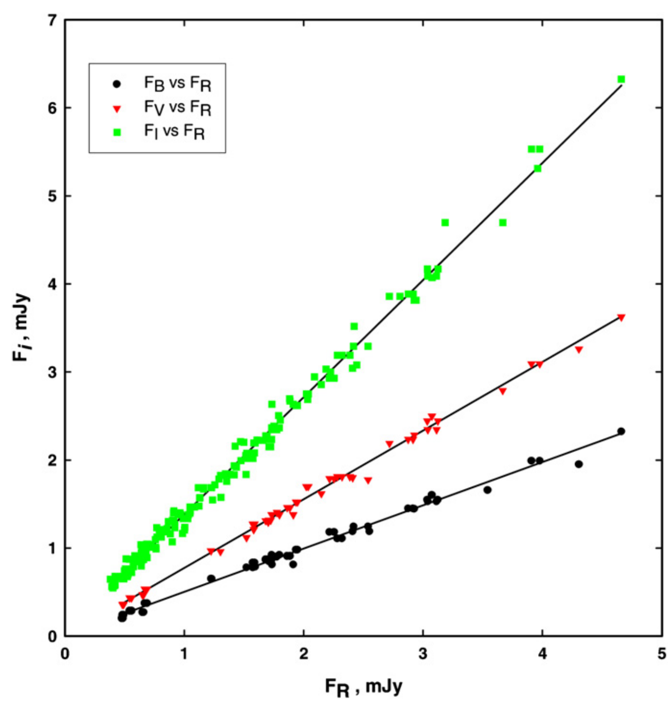

Figure 4. Dependences of the flux in the B, V, and I bands on the flux in the R band (the fluxes are corrected for the Galactic extinction). The lines represent linear regression fits to the dependences.

(A color version of this figure is available in the online journal.)

We use magnitude-to-flux calibration constants for optical *BVRI* bands from Mead et al. (1990). Galactic absorption in the direction of S4 0954+65 is calculated according to Cardelli's extinction law (Cardelli et al. 1989) and $A_V = 0.38$ mag (Schlegel et al. 1998).

Figure 4 presents flux–flux dependences between values in the *BVRI* bands with the R band chosen as the primary reference band. Figure 4 shows that during the 2011 March–April flare the flux ratios follow linear dependences, $F_i = A_i + B_i \cdot F_R$, where i corresponds to the B, V, and I bands. Values of B_i, the slopes of

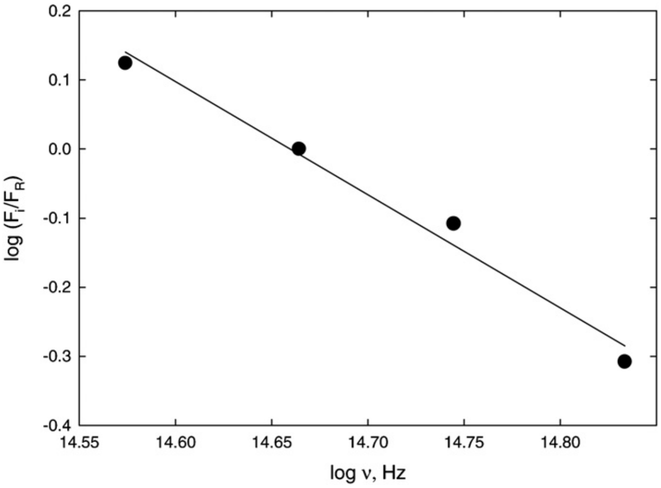

Figure 5. Relative spectral energy distribution of the variable source in S4 0954+64 obtained by using the linear regressions shown in Figure 4. The solid line represents a linear fit of the SED.

the regressions, versus the frequency of the corresponding band represent a relative SED of the variable source. As can be seen in Figure 5, on a logarithmic scale the SED is fit very well by a linear slope $\alpha = -1.64 \pm 0.15$ that suggests that the variable source emits synchrotron radiation with $F_\nu \propto \nu^\alpha$.

3.2. Radio VLBI Versus Optical and Gamma-Ray Data

Figure 1 presents the multi-frequency light curves of S4 0954+658 and optical polarization parameter curves along with an indication of times of ejection of the superluminal knots. Figure 6 shows the γ-ray light curve overlaid by the optical light curve (top panel); the degree of optical polarization and polarization of the very long baseline interferometry (VLBI) core at 43 GHz (middle panel); the position angle of optical polarization and the position angle of the VLBI core at 43 GHz (bottom panel). Similar plots that show light curves and polarization parameters' curves of other VLBI knots are available online in the electronic edition. Figure 7 shows the evolution of the distance of knots from the core, while Figure 8 displays the VLBA image of the source at 43 GHz with trajectories of the knots superposed.

We carefully study the optical polarization behavior of S4 0954+658 near the ejection times of the components. For the majority of knots (8 of 11), we have found a connection between the time of the ejection of a component and activity at the optical and radio wavelengths (37 GHz). A visual inspection of Figure 6 reveals that during most of the observational period the optical EVPA was $\chi \sim -7°$, close to the mean radio EVPA of the radio core ($-12°$) and mean jet direction ($-20°$).

A number of flares are apparent in the optical light curve during the period of observations 54800–56000 (Figure 1). Of particular interest are the flares 2, 3, 3a, 5, 5a, during which γ-ray detections occurred. To compare epochs of optical flares with the epochs of ejections of superluminal knots, we separate the sample of optical flares into two groups. Group A includes positive detections, for which $|(T_{\mathrm{opt_{max}}} - T_{\mathrm{eject}})| \leqslant \sigma$, where σ is the 1σ uncertainty in T_{eject} and group B, for which $|(T_{\mathrm{opt_{max}}} - T_{\mathrm{eject}})| \leqslant 3\sigma$. Table 5 lists the epochs of optical flares (Figure 1), epochs of γ-ray detections, the presence of optical χ rotation during each flare, the speed of optical χ rotation if

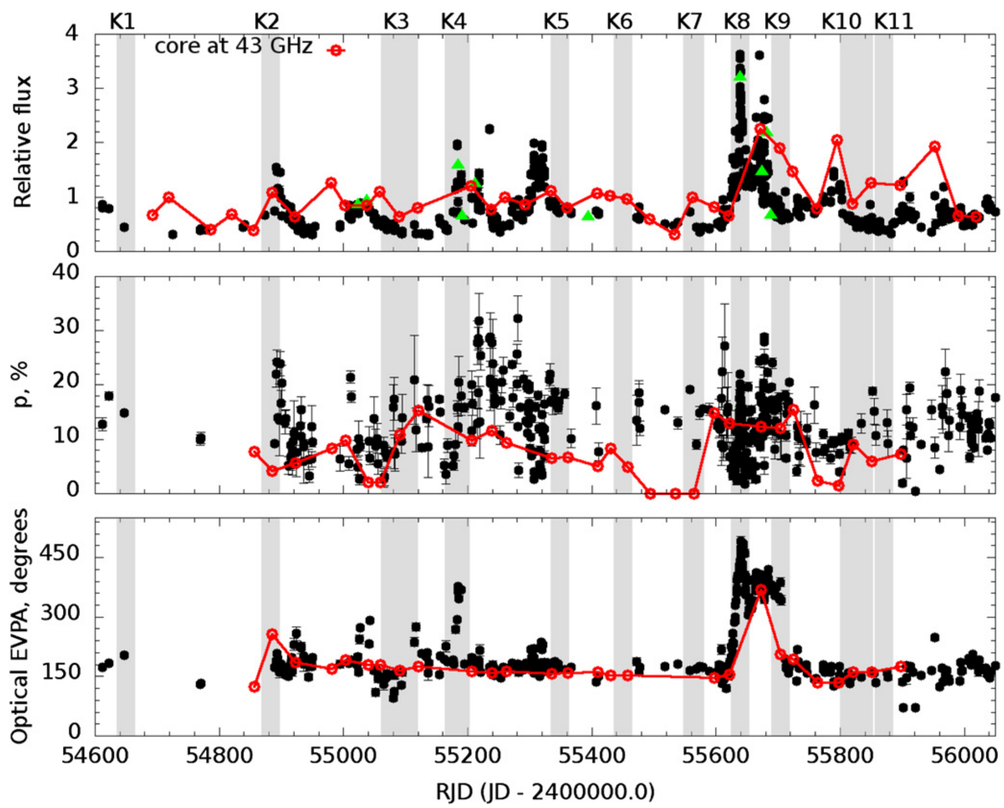

Figure 6. Top panel: optical (R-band) light curve (filled circles) overlaid by γ-ray light curve (triangles), and VLBI core light curve at 43 GHz (open circles). Middle panel: optical fractional polarization vs. time curve (filled circles) overlaid by P of the VLBI core vs. time curve (open circles). Bottom panel: position angle of optical polarization vs. time curve overlaid by EVPA of the VLBI core vs. time curve (open circles).

(A color version and extended version of this figure are available in the online journal.)

Table 5
The Summary of Optical Flares

N	Optical Flare RJD	γ-Ray	Optical χ "Rotation" (°)	Speed of Optical χ "Rotation" (° day^{-1})	Knot Ejection	Type	Connection Flare–Knot
1	54891.807	...	...	...	K2	A	?
2	55020.307	Y	27	4.5	K3	B	Yes
3	55182.447	Y	180	15.7	K4	A	Yes
3a	55217.384	Y	...	...	K4	B	?
4	55319.363	...	...	...	K5	B	?
5	55637.580	Y	333	13.3	K8	A	Yes
5a	55669.434	Y	...	...	K9	B	?
6	55789.258	...	...	...	K10	B	?
7	55900.574	...	...	...	K11	B	?

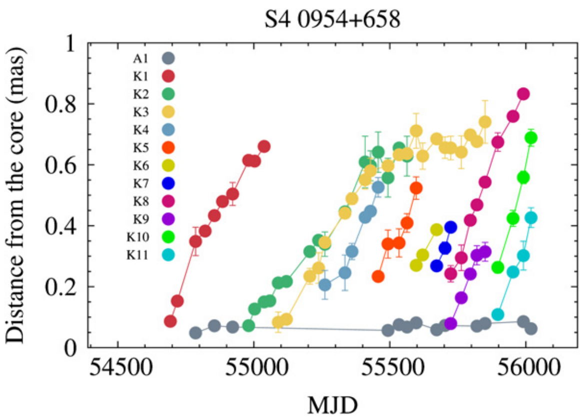

Figure 7. Separations of knots from the core as a function of time.
(A color version of this figure is available in the online journal.)

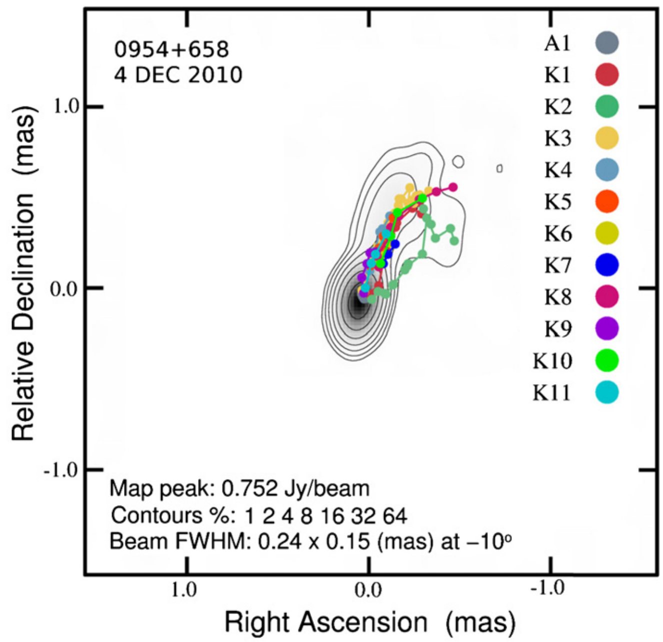

Figure 8. 43 GHz image of the source with trajectories of knots superposed.
(A color version of this figure is available in the online journal.)

rotation is found, the epoch of knot ejection if detected, and the type of the flare according to classification introduced above.

Component K1. Knot K1 is very bright, but we do not have enough data at optical wavelengths for a detailed analysis. Nevertheless, the 37 GHz light curve shows a strong flare that precedes the ejection time of knot K1 within 1σ uncertainty of $T_{\rm eject}$.

Component K2. The ejection of knot K2 was simultaneous with an optical flare and an increase of the optical polarization up to 24% within 1σ uncertainty of $T_{\rm eject}$. Although there are a number of short rotations of the optical EVPA within 3σ uncertainty of $T_{\rm eject}$ of K2, we have too few measurements ($\leqslant$4 points) to follow the EVPA evolution well in these cases.

In addition, the position angle of K2 ($\langle\Theta\rangle = -49°$) is quite different from the mean jet direction ($\sim -20°$). Before the ejection of K2, we see a modest flare in the core (RJD = 54885), which coincides with the optical flare 1 (see Table 5). During the flare, the EVPA of the core is ~76°, which differs significantly from both the mean optical EVPA and the mean EVPA of the core ($\sim -12°$). There is a sharp jump in the optical EVPA at RJD ~ 54923 with χ varying from 78° to 45°. The latter agrees with the EVPA of K2 ($\chi = 45°$) at RJD = 54981, when the knot is first resolved from the core at the VLBA images. This suggests a connection between the optical and radio events.

Component K3. The appearance of knot K3 was accompanied by a ~27° rotation of the optical EVPA (RJD 55063–55068, ~4.°5 day^{-1}) within 1σ uncertainty of $T_{\rm eject}$. In addition, a broad flare in the R band with maximum at RJD 55024 was contemporaneous with the ejection of K3 within 3σ uncertainty of $T_{\rm eject}$, as well as with two detections in γ-rays.

Component K4. The ejection of K4 was accompanied (within 1σ of $T_{\rm eject}$) by a ~180° rotation of the optical EVPA (~15.°7 day^{-1}), an increase of the fractional polarization up to 20%, an optical flare, a flare in the VLBI core and at 37 GHz (RJD 55192 $S = 2.17 \pm 0.14$ Jy), and three detections at γ-ray energies. Also, the historical maximum level of the optical fractional polarization (RJD = 55217, $P = 41\%$) was achieved within 2σ uncertainty of $T_{\rm eject}$.

Component K5. The ejection of K5 was contemporaneous with an optical flare at RJD 55319 ($S_R = 1.96$ mJy, $P = 12\%$). At the time when K5 was emerging from the core, we did not find significant smooth rotation of the EVPA, but we detected an increase of the optical fractional polarization in the form of a plateau with a mean value of ~17%, and a strong flare at 37 GHz.

Components K6 and K7. Knots K6 and K7 are weak and were detected only at three epochs. However, knot K7 is seen clearly in the polarization maps (see Figure 9). We have not found contemporaneous violent activities in the optical and γ-ray bands, which can be associated with these components similar to those of K2–K5.

Component K8. The most interesting is knot K8, whose appearance coincides within 1σ uncertainty with the major flare

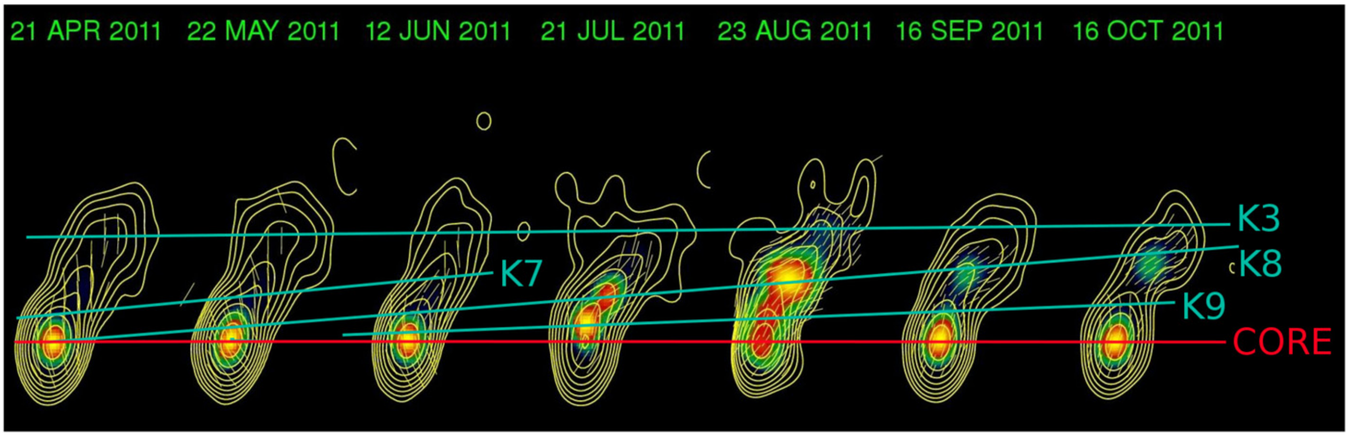

Figure 9. Total (yellow contours) and polarized (color scale) intensity images at 43 GHz; yellow line segments over the color scale show the direction of the electric vector.

(A color version of this figure is available in the online journal.)

in the R-band light curve, a flare at γ-ray energies, a strong flare in VLBI core and at 37 GHz. The emergence of knot K8 from the core was also accompanied by a significant rotation of the optical EVPA ($\sim$330°, $\sim$13.°3 day^{-1}), and by a high level of optical fractional polarization, up to 22%.

Component K9. Violent intranight variability, observed during the night of 2011 April 24 (brightening by $\sim$0.7 mag within 7 hr), was contemporaneous with the ejection of knot K9 within 2σ uncertainty of $T_{\rm eject}$. During this flare, the flux in the R band increased up to 2.47 mJy and the degree of optical polarization rose up to 28%.

Component K10. Knot K10 was ejected after a flare in the R-band light curve at RJD = 55789 (within 2σ uncertainty of $T_{\rm eject}$), which was also contemporaneous with a flare at 37 GHz (RJD = 55786, S = 1.66 Jy) and a flare in VLBI core, while a moderate degree of both optical ($\sim$10%) and VLBI core polarization ($\sim$2%) was observed during the flare.

Component K11. Knot K11 passed through the core within 2σ uncertainty of $T_{\rm eject}$ before a flare in the R-band light curve at RJD = 55900. We have not found contemporaneous violent activities in optical and γ-ray bands.

The feature A1 is detected at many epochs during our VLBI observations at a stable position of 0.07 ± 0.01 mas with respect to the core (see Figure 7). Jorstad et al. (2001) found that "stationary hot spots" are a common characteristic of compact jets, with the majority of such features located within a range of projected distances of 1–3 pc from the core. These authors proposed three categories of models for stationary components in supersonic jets: (1) standing recollimation shocks caused by imbalances between the pressure internal and external to the jet; (2) sites of maximum Doppler beaming where a bent jet points most closely to the line of sight; and (3) stationary oblique shocks, where the jet bends abruptly. We consider that knot A1 most likely falls in category (1), since it is quasi-stationary with an observed "lifetime" at least several months.

3.3. Statistical Analysis of Coincidences between Optical Flares and Ejections of VLBI Knots

We carried out numerical simulations in order to determine the probability of random coincidences between epochs of optical flares and ejection of superluminal knots in the same manner as described in Jorstad et al. (2001). We fixed the number and epochs of optical flares according to Table 5 and

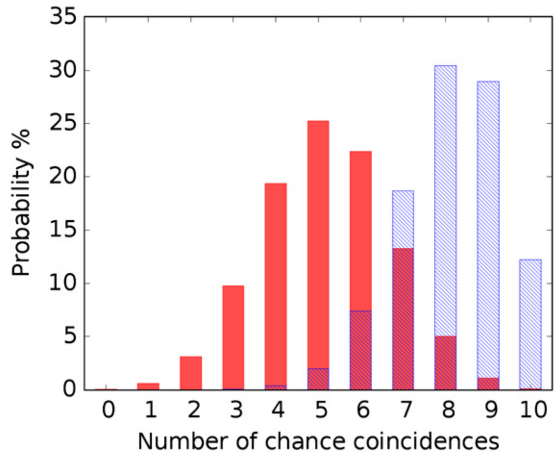

Figure 10. Probability of chance coincidences between optical flares and epochs of zero separation within 1σ (dark shading) and 3σ (light shading) uncertainties.

(A color version of this figure is available in the online journal.)

generated 1,000,000 samples of random epochs of ejections of VLBI superluminal components. Each sample consists of 10 random ejections (we do not include knot K1, which was ejected before the beginning of the optical and γ-ray monitoring). We set the uncertainties of generated epochs of zero separations equal to the uncertainties of observed superluminal ejections. A coincidence was registered in the same manner (groups A and B) as discussed above. In our observations, we found three coincidences of group A and six of group B (see Table 5). Figure 10 shows the results of the numerical simulations, which demonstrate that the probability of having three or more coincidences within 1σ is more than 80%. The probability of having nine or more coincidences within 3σ (including three coincidences within 1σ) is $\sim$40%. These values are too high to provide any meaningful constraints. An increase of the probability of chance coincidences with number of ejections is caused by two factors: (1) a significant number (10) of ejections during the relatively short observational interval of $\sim$1100 days (RJD 54850−55950), and (2) the sufficiently large mean value of a 3σ uncertainty of $\sim$57 days for one component, which corresponds to a half of the observational interval for 10 components.

Although there is a quite high probability that the optical flares and ejections of VLBI knots are not connected, it is essential to note that we use more than one criterion to associate optical flares with the appearance of superluminal knots. These include the relation between optical and radio polarization measurements, connection with detections of S4 0954+658 in γ-rays. We consider with confidence that components K8 and perhaps K4 and K3 are associated with optical flares (5, 3, and 2, respectively) due to similarity in the optical/radio polarization behavior during the flares and structure of the γ-ray outbursts, which can be related to the structure of the inner jet.

We cannot exclude that the γ-ray flares RJD $\sim$ 55210 and RJD $\sim$ 55680 (near optical flares 3a and 5a, respectively) may still be associated with the propagation of K4 and K8 down the jet. An interaction of the knots with the standing recollimation shock associated with A1 could lead to the second γ-ray flare and optical intranight variability, similar to the case observed in the quasar 3C 454.3 (Jorstad et al. 2013). According to the proper motion, K8 should reach A1 in 30 $\pm$ 15 days, which is similar to the time lapse between the first and second γ-ray flares, $\sim$42 days. So the knot K9 may in fact be a new component generated after the interaction of K8 and A1. A similar case is observed for component K4 and γ-ray flare RJD $\sim$ 55210 (contemporaneous with optical flare 3a): knot K4 should reach A1 in 41 $\pm$ 21 days, while the time lapse between flares is $\sim$30 days.

4. CONCLUSIONS

The BL Lac object S4 0954+658 has displayed very prominent optical activity starting from 2011 mid-February. Our photometric and polarimetric observations densely cover this period. In addition, we have an impressive set of VLBA images at 43 GHz that allows us to compare optical activity with the behavior of the parsec-scale jet. We conclude the following.

1. During the entire interval of our observations the source exhibited violent variability in optical bands and a high level of activity in the jet at 43 GHz. We follow the ejection of new components with a rate $\sim$3 new knots per year. It should be noted that not many blazars show such a high frequency of ejections of superluminal knots, comparable with the scale of optical activity.
2. During the interval from RJD 54800−55900, we have identified nine strong optical flares. Out of these nine events, four were contemporaneous with positive detections of γ-ray emission at a flux level exceeding 5×10^{-7} photons cm^{-2} s^{-1}. Only one detection at γ-rays was not associated with an optical flare.
3. The overall behavior of the source during the most prominent optical outburst in 2011 March–April can be explained as a superposition of radiation of a long lived component with constant Stokes parameters and a new, strongly variable one whose EVPA rotates at a rate of $\sim 13^\circ$ day^{-1} from the onset of the outburst until the moment of maximum flux and then levels at $\sim 310^\circ$. Corrected for $k \cdot 180^\circ$ ambiguity, this is equivalent to -50°, which is quite different from the pre-outburst direction (-6°). This fast and monotonic rotation might be explained as the spiral motion of the variable source in a helical magnetic field (a new superluminal knot; Marscher et al. 2008, 2010; Larionov et al. 2013). The VLBA images at 43 GHz show the ejection of a new, highly relativistic knot, K8, coincided within 1σ uncertainty of T_{eject} with the major peak in the R-band light curve, a flare at γ-ray energies, and a flare in VLBI core and at 37 GHz.
4. According to our optical data, the polarization parameters of the variable source ($p = 27\%$, $\chi = -25^\circ$, "c" in Table 4) are close to the polarization parameters of K8 ($p = 27\%$, $\chi = -34^\circ$; see Table 2) at the epoch (2011 June 12) when it was first separated from the core at the 43 GHz images (set of Figures 6). The knot preserved a high level of fractional polarization at later epochs.
5. According to our analysis, 8 of 11 superluminal components (K2, K3, K4, K5, K8, K9, K10, K11) emerged during strong optical flares (within 1σ–3σ uncertainty of T_{eject}). However, the Monte Carlo simulation indicates that there is no evidence from the timing of the optical flares and VLBI ejecta alone to support the claim that the two are related. We have very strong evidence to connect one superluminal component (K8) to a near-simultaneous optical flare, and some evidence of connections between at least two more (K4 and K3) superluminal ejecta and near-simultaneous optical flares.
6. The γ-ray outbursts, which can be associated with knots K4 and K8 based on T_{eject} (Figure 1), reveal a double structure that might be explained by the interaction of a moving knot with the two stationary features in the inner jet, the core A0 (the first peak) and knot A1 (the second peak), which are presumably standing recollimation shocks.
7. High-amplitude intranight variations were detected in both optical light and fractional polarization. This may reflect fine structure of the magnetic field, as would be expected, e.g., if the jet plasma is turbulent (Marscher 2014).
8. We have found three cases of smooth optical EVPA rotation that are associated with component ejections (see Table 5) at high confidence supported by our well-sampled optical and VLBA data. The slowest rate of the optical EVPA rotation occurs during the appearance of knot K3, whose apparent speed was a factor of two slower than the average speed of superluminal knots in the jet. However, we cannot say that this is a common pattern without more data.
9. During the interval of our observations, the highest flux level of the VLBI core at 43 GHz was contemporaneous with the major optical outburst. A high level of fractional polarization ($\sim$13%) was seen in the core during the optical flare and dropped to 2% after the outburst. A lower level of fractional polarization at 43 GHz with respect to the optical degree of polarization may be due to a larger volume of the region radiating at 43 GHz and turbulent magnetic field. In addition, the polarization position angle of the core and almost all of the components was close to the mean jet direction, as was the optical EVPA in quiescent states (see set of Figures 6). This implies that the magnetic field in the regions of optical and radio emission has similar structure. Moreover, a simultaneous increase of the degree of optical polarization and that of the core leads to the conclusion that the two regions are co-spatial.

We thank anonymous referee for useful comments and suggestions. This work was partly supported by Russian RFBR grants 12-02-00452, 12-02-31193, 13-02-00077, St. Petersburg University research grants 6.0.163.2010, 6.38.71.2012, and by NASA Fermi Guest Investigator grants NNX08AV65G, NNX11AQ03G, and NNX12AO90G. The VLBI data were obtained within the program VLBA-BU-BLAZAR. The VLBA is an instrument of the National Radio Astronomy Observatory. The National Radio Astronomy Observatory is a facility of the National Science Foundation operated under cooperative agreement by Associated Universities, Inc. The PRISM camera at Lowell Observatory was developed by K. Janes et al. at BU and the Lowell Observatory, with funding from the National Science Foundation, BU, and the Lowell Observatory. The Liverpool Telescope is operated on the island of La Palma by the Liverpool John Moores University in the Spanish Observatorio del Roque de los Muchachos of the Instituto de Astrofisica de Canarias, with financial support from the UK Science and Technology Facilities Council. This paper is partly based on observations carried out at the German–Spanish Calar Alto Observatory, which is jointly operated by the MPIA and the IAA-CSIC. Acquisition of the MAPCAT data is supported by MINECO (Spain) grant and AYA2010-14844, and by CEIC (Andalucía) grant P09-FQM-4784. The Metsähovi team acknowledges support from the Academy of Finland to their observing projects (212656, 210338, 121148, and others) This work was partly carried out using computer resources provided by Resource Center "Computer Center of SPbU" (http://cc.spbu.ru).

REFERENCES

Abdo, A. A., Ackermann, M., Ajello, M., et al. 2010, ApJS, 188, 405
Atwood, W. B., Abdo, A. A., Ackermann, M., et al. 2009, ApJ, 697, 1071
Cardelli, J. A., Clayton, G. C., & Mathis, J. S. 1989, ApJ, 345, 245
Gabuzda, D. C., Kochenov, P. Y., Kollgaard, R. I., & Cawthorne, T. V. 2000, MNRAS, 315, 229
Hagen-Thorn, V. A., Larionov, V. M., Jorstad, S. G., et al. 2008, ApJ, 672, 40
Hagen-Thorn, V. A., & Marchenko, S. G. 1999, BaltA, 8, 575
Jorstad, S. G., Marscher, A. P., Lister, M. L., et al. 2005, AJ, 130, 1418
Jorstad, S. G., Marscher, A. P., Mattox, J. R., et al. 2001, ApJS, 134, 181
Jorstad, S. G., Marscher, A. P., Smith, P. S., et al. 2013, ApJ, 773, 147
Kudryavtseva, N., Gabuzda, D., Mahmud, M., & O'Sullivan, S. 2010, in 10th European VLBI Network Symposium and EVN Users Meeting: VLBI and the New Generation of Radio Arrays, 45
Larionov, V. M., Jorstad, S. G., Marscher, A. P., et al. 2011a, in 2011 Fermi Symp., ed. A. Morselli, eConf C110509
Larionov, V. M., Jorstad, S. G., Marscher, A. P., et al. 2013, ApJ, 768, 40
Larionov, V. M., Morozova, D. A., Troitsky, I. S., et al. 2011b, ATel, 3220, 1
Marscher, A. P. 2012, IJMPS, 8, 151
Marscher, A. P. 2014, ApJ, 780, 87
Marscher, A. P., Jorstad, S. G., D'Arcangelo, F. D., et al. 2008, Natur, 452, 966
Marscher, A. P., Jorstad, S. G., Larionov, V. M., et al. 2010, ApJL, 710, L126
Mead, A. R. G., Ballard, K. R., Brand, P. W. J. L., et al. 1990, A&AS, 83, 183
Mukherjee, R., Aller, H. D., Aller, M. F., et al. 1995, ApJ, 445, 189
Nesterov, N. S., Volvach, A. E., & Strepka, I. D. 2000, AstL, 26, 204
Nolan, P. L., Abdo, A. A., Ackermann, M., et al. 2012, ApJS, 199, 31
Raiteri, C. M., Villata, M., Tosti, G., et al. 1999, A&A, 352, 19
Schlegel, D. J., Finkbeiner, D. P., & Davis, M. 1998, ApJ, 500, 525
Teraesranta, H., Tornikoski, M., Mujunen, A., et al. 1998, A&AS, 132, 305
Wagner, S. J., Witzel, A., Krichbaum, T. P., et al. 1993, A&A, 271, 344